J Mater Sci (2016) 51:8861–8879

New colloidal fabrication of bioceramics with controlled porosity for delivery of antibiotics

Lydie Ploux[1,*], Mihaela Mateescu[1,2], Lise Guichaoua[2], Jules Valentin[1], Judith Böhmler[1], Karine Anselme[1], Eric Champion[2], Nathalie Pécout[2], Roxana Chotard-Ghodsnia[2], and Marylène Viana[2]

[1] *CNRS/Université de Haute Alsace/Université de Strasbourg - Institut de Science des Matériaux de Mulhouse (UMR7361), 15 rue Jean Starcky, BP2488, 68057 Mulhouse cedex, France*

[2] *Université de Limoges, CNRS, ENSCI, SPCTS, UMR7315, 87000 Limoges, France*

Received: 30 November 2015
Accepted: 11 June 2016
Published online: 28 June 2016

ABSTRACT

Bone tissue regeneration with bioceramics-based biomaterial can suffer from associated bone infections. The objective of this study was to develop new antibiotics drug delivery systems, composed of ceramics matrix with a controlled porosity aiming at releasing the antibiotics loaded in the matrix, in the bone implantation site and in a controlled way. Synthesis of the ceramics matrix is based on a colloidal approach. First, the heterocoagulation of hydroxyapatite nanoparticles (HA) and polymethylmethacrylate microspheres (PMMA) provides the control of the porosity in HA matrix. With constant size of microspheres and HA/PMMA ratio, the sintering temperature allows the modulation of interconnections porosity and volume. In this study, two sintering temperatures, resulting in two different porosities, are used. Secondly, porous biomaterials are loaded with tetracycline hydrochloride (antibiotics with large spectrum used in treatment of bone infections) by impregnation under vacuum. Control of the porous microstructure allows variation of the loaded quantity of antibiotics and of their release kinetics. The antibacterial properties of the ceramics loaded with antibiotics vary with the porous microstructure, both in terms of bacterial growth in the ceramic surroundings and of bacterial colonization of the ceramic surface. Protein adsorption from surroundings onto the ceramic surface varies depending on the porous structure, however without inducing significant changes of antibacterial properties. Unloaded and loaded porous bioceramics are biocompatible with pre-osteoblastic cells as shown by in vitro evaluation. The investigation of DDS with two different porosities demonstrated the possibility to control the antibiotics loaded quantity and the antibacterial efficiency by varying the matrix porosity. Release kinetics is also affected by changes in ceramic porosity but in a much more limited way.

Roxana Chotard-Ghodsnia—In memoriam.

Address correspondence to E-mail: Lydie.Ploux@uha.fr

DOI 10.1007/s10853-016-0133-z

Introduction

Infections on biomaterials are a common cause of implantation failure often forcing the removal of the infected material [1]. Biomaterial-associated infections are due to bacterial biofilms developed on the implant surface after initial contamination occurring during surgery or due to bacteria coming from infections in the patient body (e.g. dental infections). Mostly, systemic antibiotic treatment is ineffective since biofilms provide protection for bacterial cells through restrictions in molecule diffusion and bacteria sensitivity [2]. Then, infections become chronic. The development of new antibacterial and anti-biofilm strategies is needed for fighting locally against biofilm growth. In this framework, bioactive biomaterials able (i) to release antimicrobial drugs with a predictable kinetics, (ii) to deliver drug in a specific location with a controlled local drug concentration and (iii) to limit adverse systemic effects by allowing reduction of the delivered doses of drug, are of major interest.

For bone tissue regeneration, hydroxyapatite (HA) is a common and well-known biomaterial. Hydroxyapatite-based ceramics materials providing antibacterial effect through antibiotic release have been proposed for designing implantable drug delivery system (DDS) [3–8]. In these bioactive materials, selection of the most suitable ceramic matrix is crucial but difficult. In particular, pore size and structure of the inorganic host system are key factors for controlling both quantity and release kinetics of the drug [9–17]. Various techniques exist for the fabrication of porous ceramics. They can be classified into 2 categories. The first one is an additive manufacturing technique based on layer-by-layer building of 3D scaffolds from a computer-aided design file [18–20]. The second approach, based on a colloidal process, is more conventional and consists in the generation of porosity inside the ceramic through various routes [21, 22]. One possibility is the impregnation of a cellular template (e.g. polyurethane foam) with ceramic suspension, before elimination of the template by a thermal treatment, providing the positive replica of the template [23]. Another method is based on the incorporation of a porogen agent that is finally eliminated by thermal treatment or dissolution [24–26], resulting in the porous ceramic. In a third method (direct foaming), porous materials are produced by incorporating air into the ceramic suspension [27, 28]. In general, versatility of these colloidal methods for the control of porosity is low, leading to pores with irregular size and spatial distribution. Here, we focus on a process using heterocoagulation, which allows the control of pore size, pore distribution in the massive material and volume of porosity [29, 30]. Micropores are expected to be obtained thanks to the presence of polymethylmethacrylate (PMMA) microspheres in a suspension of HA nanoparticles. Pore size is controlled by the size of the microspheres, while homogeneity of pore distribution results from the dispersion of the initial HA/PMMA suspension. Porosity can be varied by adapting the volumic ratio between HA particles and PMMA spheres [31].

Our first objectives were the synthesis of HA-based ceramics with a controlled porosity, and the control of loading and in vitro release of antibiotics thanks to control of the porous microstructure. Two different microstructures were chosen for their good compromise between interconnection rate and matrix cohesion/stability allowing to expect satisfying mechanical properties [32]. They were loaded by in-vacuum impregnation [16] with tetracycline hydrochloride (TC), a large spectrum antibiotics used for bone infection treatments [33]. Our second objective was to investigate the antibacterial properties of these new DDSs and to confirm their biocompatibility for mammalian cells.

Here, HA matrices with two different microstructures will be described, especially in terms of porosity (pore rate, pore size distribution, and interconnections). Their properties as DDS will then be investigated based on their ability to adsorb and release TC. In a second part, the antibacterial properties of the DDS will be reported. Short- and middle-term antibacterial effects for both bacteria in the near surrounding of the DDS and bacteria adherent to the material will be addressed in particular. Additionally, in vitro biocompatibility of the developed DDS was evaluated on eukaryotic cells. Since implantable biomaterials are usually suited in complex surroundings such as body fluids, they are subject to the adsorption of a large range of biochemical components, including proteins for a large part, which may rapidly condition their surface before mammalian cells and bacteria adhere [34]. Adhesion of mammalian cells and bacteria may thus be affected by changes in chemical properties of the

material surface. In addition, adsorbed components of the conditioning film may affect delivery properties of the DDS by forming a barrier and preventing bioactive agent release. In this frame, biomolecules in cell culture medium are expected to adsorb onto HA-1100 and HA-1220 DDS. The potential barrier effect of proteins previously adsorbed onto the HA surface has been therefore investigated and will be here briefly discussed.

Materials and methods

Preparation and characterization of porous materials (HA DDS): heterocoagulation process

Preparation and characterization of the porous materials are described elsewhere [29]. Briefly, microspheres of polymethylmethacrylate (PMMA) were used as a structuring agent (Fig. 1a). Mean diameter of spheres was 7 μm and zeta potential was −30 mV at pH 6.6 in aqueous medium. Powder of stoichiometric hydroxyapatite (HA, Fig. 1b) was synthesized by co-precipitation in aqueous medium, as previously described [35]. It was then re-suspended in aqueous medium, dispersed and stabilized by addition of polycationic dispersant. Mean size of hydroxyapatite particles dispersed in suspension was 0.1 μm and zeta potential was +50 mV between pH 6 and 7. Suspensions of HA and PMMA were mixed at a HA/PMMA ratio of 0.42 as previously determined [31]. The resulting suspension was filtered to remove solvent. Pressure created by pumping caused the compaction of HA/PMMA particles, leading to the formation of thin cylinders (~12 mm in diameter and 1–2 mm in thickness) of an organic/inorganic composite. Drying of the composite material was achieved in oven before thermal treatment at 500 °C aiming at the removal of the PMMA microspheres. The material was finally sintered at 1100 or 1220 °C to provide final ceramics with two different porosities (materials named HA-1100 and HA-1220, respectively). The resulting material samples were thin cylinders of 11.4 ± 0.5 mm in diameter and 1.2 ± 0.3 mm in thickness. The porous microstructure of the final materials was confirmed by Scanning Electronic Microscopy (Hitachi S2500). Pores and interconnections characteristics (rate and size) were determined using mercury porosimetry (Micromeritics Autopore 9510). Three different HA samples were used

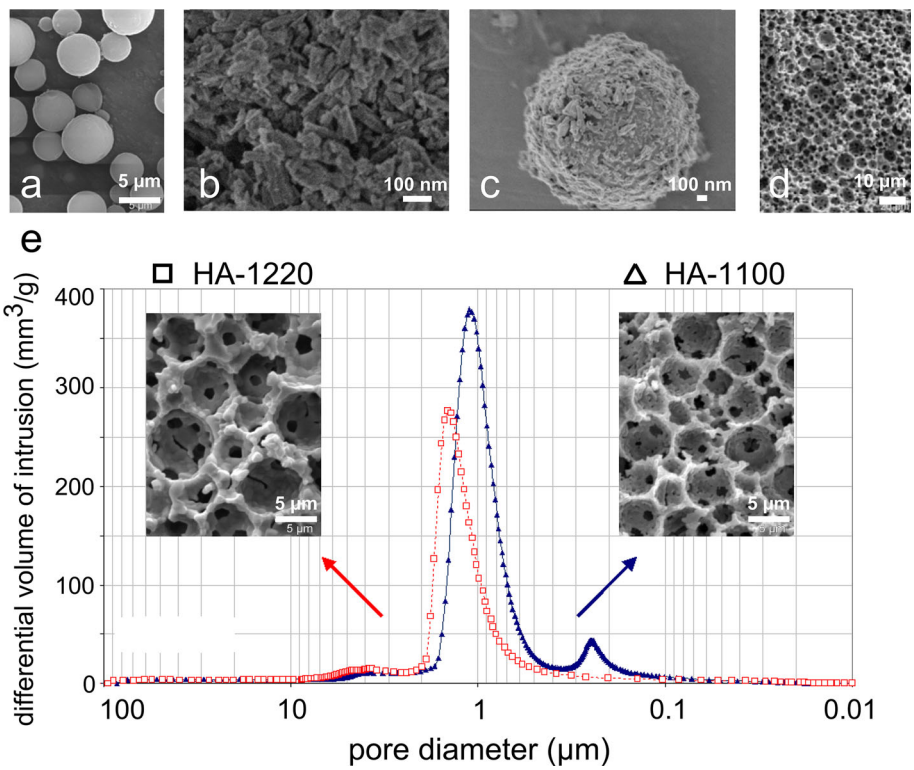

Figure 1 **a** PMMA microspheres, **b** hydroxyapatite (HA) nanoparticles, **c** PMMA microspheres coated by HA nanoparticles, **d** porous ceramics after sintering, **e** porogram and SEM micrographs of porous ceramics synthesized with a 0.42 HA/PMMA volume ratio and sintered at 1100 °C (HA-1100) and 1220 °C (HA-1220).

together to provide one measurement and measurement was carried out once. Porosity was also calculated on the basis of weight, area, and thickness of the HA samples according to Eq. 1, where HA density is 3.065 g/cm^3. This porosity was determined for each sample.

$$\text{Porosity}(\%) = \left(1 - \frac{\text{Weight}}{\text{Area} \times \text{Thickness} \times \text{HA density}}\right) \times 100 \quad (1)$$

Preparation and characterization of porous materials loaded with tetracycline (TC-HA DDS)

Tetracycline hydrochloride (TC) (Supporting Information, Fig. 1a; MIC_{50} of 1–16 μg/mL for *Escherichia coli* (*E. coli*) [36]) was purchased by Cooper (Melun, France) as a yellow powder. Porous ceramics were impregnated under vacuum conditions with solutions of TC in ethanol during 30 min, before drying in air at 37 °C. Concentrations of TC in ethanol ranged from 5 to 15 mg/mL. For each of these initial concentrations, the quantity of TC loaded in the porous ceramics was determined by using UV-spectrophotometry (Lambda 25, Perkin Elmer) at 276 nm after achievement of total dissolution of TC-HA samples in acid solution (HCl, 2.4 M). For the concentration finally used for biological assays (5 mg/mL of tetracycline in ethanol), measurement of TC quantity in porous ceramics was also achieved by Temperature Programmed Desorption, as described in Gadiou et al. [37]. Tetracycline degradation fragments with $m/z = 50$, that may be the result of various pathways of the complex degradation of TC [38–41], were used as a signature of the tetracycline molecules loaded in HA matrix. A calibration curve was provided in a range of TC quantity from 0 to 2.5 mg (Supporting Information, Fig. 1b). Results are presented as the mean value ± standard deviation of at least three replicates for the first method, two replicates for the second method.

In order to investigate the incidence of the porous structure of the HA matrix, the property of release of the DDS was assayed on TC-HA-1220 and TC-HA-1100 containing the same quantity of adsorbed TC molecules. For that purpose, the kinetics of TC release were determined in aqueous medium and under controlled conditions (50 mL of water, continuous stirring, pH 7, $T = 37$ °C). Assaying by using UV-spectrophotometry (Lambda 25, Perkin Elmer) at 276 nm provided the concentration of dissolved tetracycline. Kinetics curves of TC release from porous materials are finally expressed as percent of released TC compared to the total mass of TC loaded in the material, determined by total dissolution as described above.

All incubation steps of biological and microbiological assays were performed in the dark to avoid any photo-degradation of tetracycline molecules.

Bacterial species and growth conditions

Before microbial characterization, samples were sterilized by UV of 254 nm wavelength during 7 min at 2 cm from UV-C lamp.

Gram-negative *E. coli* were chosen as a model for pathogenic bacteria species among the most frequently implicated in implant-associated infection [42–44]. Experiments were conducted with *E. coli* PHL628 (*E. coli* MG1655) known to produce curli and exocellular polymeric substances and to attach to abiotic surfaces [45]. After defrosting of 1 mL of bacteria stored at −80 °C, three successive pre-cultures were grown at 30 °C (10 % vol. of the previous pre-culture in fresh medium). Both first steps of pre-culture were grown overnight whilst the last one was grown for 4 h and was used to inoculate the final culture (10 % vol. of the last pre-culture). All bacterial cultures were done in a selective medium (M63G [45], pH 6.8) to avoid any uncontrolled adsorption of biomolecules coming from the medium. Concentrations of bacteria in aqueous suspensions were determined by absorbance measurements at 600 nm (Abs_{600nm}) under UV–visible spectrometer. Abs_{600nm} were then converted in number of bacterial per volume by using adequate calibration relationships.

Adhesion inhibition of bacteria onto DDS and growth inhibition of adhered bacteria

The ability of TC-HA DDS to inhibit in vitro bacterial adhesion and/or growth of bacteria adhered on DDS surface was evaluated by measuring the adhered bacterial population and estimating their cultivability. Sterilized samples were inoculated with 4 mL of M63G medium containing 5×10^6 bacteria/mL ($Abs_{600nm\ initial}$ of 0.01) and incubated for 2 h at 30 °C. Then, samples were rinsed three times with 2 mL of

fresh NaCl solution (9 g/L in water) to collect non-adherent bacteria without creating any air-material interface [46]. Abs_{600nm} of initial supernatants (i.e. supernatants after 2 h of culture) and of rinsing solutions (Supporting Information, Fig. 2) were measured and were summed for each sample to assess the amount of planktonic bacteria after culture. Corresponding inhibition rates were measured by $(Abs_{600nm\ initial} - Abs_{600nm})/Abs_{600nm\ initial}$. These inhibition rates are called "Inh_{plank1}" in the following. Assays were repeated 5 times for each HA and TC-HA DDS. Results are given as the average of the replicates. After NaCl 9 g/L rinsing, HA and TC-HA DDS samples were used for the evaluation of quantity and cultivability of adhered bacteria.

Bacterial colonization on DDS samples was analysed in situ in the last NaCl 9 g/L rinsing solution by using a Confocal Laser Scanning Microscope (CLSM) (Zeiss LSM700 mounted on an upright microscope and equipped for fluorescence and reflection microscopy modes) equipped with a water immersion objective (W Plan Apochromat ×63/1.0) for keeping bacteria in satisfying physiological conditions. 3D images were performed with the reflection mode for allowing characterization of the material surface topography and with the fluorescence mode after Syto9® (Molecular Probes, 1 µL of 5 mM Syto9® stock solution per mL of NaCl) fluorescent staining for visualizing adhered bacteria. Quantity of adhered bacteria was determined after treatment of the 3D images using ImageJ software [47] and image analysis using CellC software [48]. This experiment was realized in triplicate. Two samples of each HA and TC-HA DDS type were observed for each experiment. Between five and ten random locations (102 µm × 102 µm) were imaged with CLSM on each

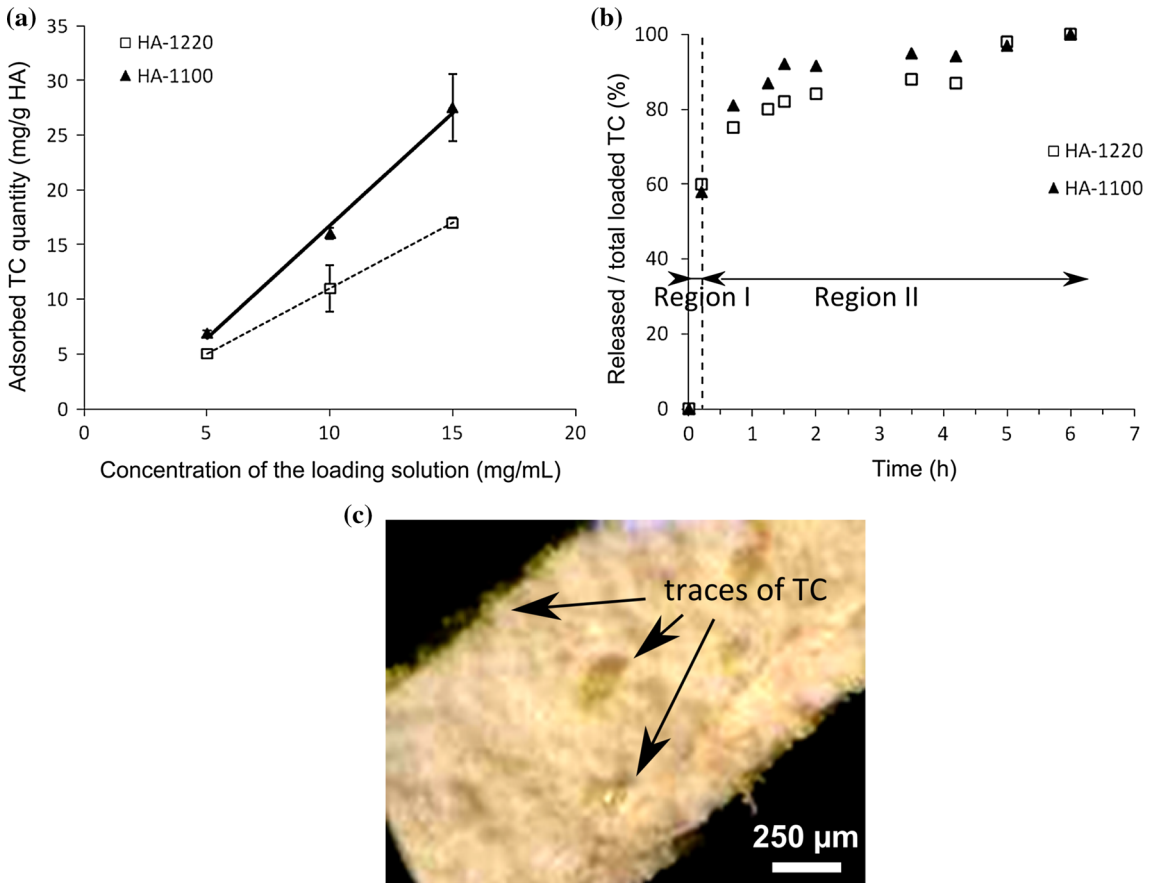

Figure 2 Behaviour of TC-HA DDS throughout TC loading and releasing. **a** Quantity of TC loaded in HA porous matrix as function of the matrix porosity and of the concentration in TC of the loading solution. **b** Kinetics of TC releasing from TC-HA DDS for 6 h in 50 mL of water, showing two different regimes of release. **c** Optical micrograph (Optical microscope MZ16, Leica) of a fractured TC-HA sample before TC releasing process, showing the presence of TC on the surface and in the inner pores of the matrices (*yellow* traces pointed out by *black arrows*).

sample. Imaging of sample border was avoided. Results are given as the average of 20–40 values. Corresponding inhibition rates are called "Inh_{adh}" in the following.

The cultivability of adhered bacteria was estimated by a so-called "print test". Sample top sides were pressed for 5 s on a LB-agar plate before removing. LB-agar plates were incubated at 30 °C for 16 h. The capacity of so-transferred bacteria to form colonies provided an indication of the cultivability of adherent bacteria. This experiment was repeated twice for each HA and TC-HA DDS type.

Growth inhibition of bacteria in DDS surroundings

Antibacterial effects of TC released from DDS on bacteria present in surroundings were evaluated both in semi-solid and in liquid media, aiming at the characterization of the TC-HA DDS ability to inhibit the growth of bacteria living in the material surroundings.

The antibacterial effect on semi-solid surroundings was evaluated by measuring areas of bacterial growth inhibition around samples loaded with antibacterial agent and placed on previously inoculated agar plates (modified Agar Diffusion Method [49]). Briefly, 100 µL of fresh bacterial suspension was spread on lysogeny broth (LB) agar-supplemented (15 g/L) growth medium to form a thin film of bacterial suspension. Sterilized HA DDS and TC-HA DDS samples were placed in contact with the previously homogenously inoculated agar plate (top side of samples in contact with agar). After 24-h incubation at 30 °C, diameters of zones without growing of bacteria (so-called Inhibition Zones, visible around TC-HA DDS samples) and diameters of the samples were measured to allow further determination of the inhibition areas. Experiment was run three times for each HA type (one HA DDS sample and the corresponding TC-HA DDS sample per agar plate). Results are given as the average of the three replicates.

Aside from the measurements performed in the supernatants of samples used for adhesion experiments (Inh_{plank1}, see section above), the antibacterial effect in liquid surroundings was also evaluated by determining the inhibition rates of growth of planktonic bacteria in the presence of DDS in culture medium for durations up to 7 days. Sterilized samples were placed in 22 mL of M63G medium containing 5×10^6 CFU/mL bacteria (Absorbance at 600 nm − $Abs_{600nm\ initial}$ of 0.01) and incubated for various periods (1, 2, 8, 24, 48, 72, 168 h) at 30 °C. After incubation, 1.5 mL of suspension was taken twice and re-injected after determination of bacterial concentration, which was performed by measuring absorbance at 600 nm (Abs_{600nm}). Inhibition rate corresponding to each sample was then calculated according to $(Abs_{600nm\ initial} - Abs_{600nm})/Abs_{600nm\ initial}$. These inhibition rates are called "Inh_{plank2}" in the following. Experiment was run 5 times for each type of TC-HA DDS. Results are given as the average of the replicates.

Protein adsorption

Potential impact of protein adsorption on the TC-related antibacterial effect has been investigated. Samples of each HA and TC-HA DDS type were kept 1 h under hydrodynamic culture conditions in cell growth medium (McCoy's, Sigma-Aldrich) containing 10 % of foetal bovine serum (FBS) and 1 % L-glutamine but without any additional antibiotics for not disturbing the analysis. Samples were placed in perfusion bioreactors (Minucells and Minutissue, Germany). Medium flow through DDS samples was maintained at 2 mL/h rate [50]. Biochemical and physicochemical analyses were performed during and after dynamic experiments. Quantity of proteins in liquid medium before and after passage through DDS was measured using BCA assay (ThermoFisher Scientific). Quantity of tetracycline released from the TC-HA DDS during dynamic adsorption of proteins was estimated by measuring the absorbance value at 276 nm (Abs_{276nm}) before and after dynamic experiment. Surface morphology and chemical composition of HA and TC-HA DDS after dynamic experiment were investigated by scanning electron microscopy (SEM) and X-ray photoelectron spectroscopy (XPS) analysis. SEM images were performed using a FEI Quanta 400 microscope after gold metallization. XPS survey spectra were recorded with a gamma SCIENTA SES 200-2 spectrometer equipped with a monochromatized KR1, 2 anode (1486.6 eV) and a concentric hemispherical analyzer. Photoemitted electrons were collected at a takeoff angle of 90° from the substrate, with electron detection in the constant analyzer energy mode. The survey spectrum signal was recorded with pass energy of 500 eV. Bacterial

growth inhibition assays were finally conducted with DDS treated with 1 h of dynamic experiment by following the same procedure as previously described ("Growth inhibition of bacteria in DDS surroundings" section) at 1, 2, 8 and 24 h of incubation time. These inhibition rates are called "$Inh_{plank\ with\ proteins}$" in the following. All these analyses were done on three different samples of each HA and TC-HA DDS type except SEM and XPS analyses (one sample of each type for each characterization technique). Results are given as the average of the replicates.

Biocompatibility tests

Compatibility of TC-HA DDS with eukaryotic cells was tested for HA-1220 and TC-HA-1220 only, which were chosen for the better compactness and stability of pore walls. Experiments were conducted with MC3T3-E1 cells (immortalized pre-osteoblastic mouse cell line, kindly provided by Dr M. Hindie (Errmece laboratory, Cergy-Pontoise University, France)). All products were provided by Sigma-Aldrich in the absence of any indication to the contrary.

Biocompatibility of released compounds was tested by cell culture in HA-1220 and TC-HA-1220 extracts. According to a weight/volume ratio of 0.1 g/mL, material samples were immerged into incomplete ISCOVE's culture medium (i.e. supplemented with 1 % L-glutamine, 100 U/mL penicillin-G and 0.1 mg/mL streptomycin sulphate but without FBS). Immersion was maintained 5 days at 37 °C for allowing the total release of TC molecules from the DDS samples. The so-obtained extract solution was further used without (100 %) or with dilution in incomplete ISCOVE's medium (50 %) and supplementation with 10 % FBS. 100 and 50 % solutions were used to replace the culture medium of cells previously cultured for 24 h at 37 °C under 5 % CO_2 condition in complete ISCOVE's medium (incomplete ISCOVE's medium supplemented with 10 % FBS) in a 96-well culture plate seeded with 2×10^4 cells per well. After 24-h incubation at 37 °C, media were replaced by 100 µL of 0.5 mg/mL MTT (3-(4,5-Dimethyl-2-thiazolyl)-2,5-diphenyl-2*H*-tetrazolium bromide [51]) before 4-h incubation at 37 °C and under 5 % CO_2 condition. MTT media were then replaced by 100 µL of acidic isopropanol (300 µL HCl + 100 mL isopropanol) for 20-min incubation at 37 °C. Acidic isopropanol was detected by measurement of absorbance at 570 nm.

Reliability of HA-1220 and TC-HA-1220 DDS for the development of attached cells was investigated by direct contact culture on the material surface. 1 mL of cells in complete ISCOVE's medium (4×10^4 MC3T3-E1 cells/mL) was used to seed each material sample (3 samples of each material type). After 6, 24 and 72 h of incubation at 37 °C and under 5 % CO_2 condition, culture medium was replaced by 500 µL of PrestoBlue® solution (Molecular Probes™) and incubated for 1 h at 37 °C before absorbance measurement at 570 nm. The absence of toxicity of PrestoBlue® solution [52] allowed further analysis of cells by fluorescent staining and microscope observations. Cells were fixed with a solution of 2 % (v/v) paraformaldehyde in NaK_2P buffer for 20 min and permeabilized with 0.2 % (v/v) of Triton X-100 for 15 min. Non-specific staining was prevented by a 20-min treatment with 1 % solution of bovine serum albumin (BSA) in phosphate buffered saline. DNA in nuclei and actin filaments were stained with 4′,6′-diamidino-2-phenylindole dihydrochloride (DAPI, 100 ng/mL) and phalloidin-TRITC (0.4 mg/mL), respectively. Three locations (386 µm × 203 µm) were observed per sample by using CLSM equipped with a water immersion objective (W Plan Apochromat ×63/1.0). Number of nuclei per micrograph, average area and circularity of cells were analysed with ImageJ software [47].

Statistical analysis

All biological experiments were run at least 3 times. For all replicates, at least 2 material samples were analysed. Results are presented as average and standard deviation of all replicates. Significance of differences was tested by two-by-two bilateral Student's t tests (application conditions: independent data and equal variances assessed by F test) with significance thresholds (α) of 0.01 and 0.05. According to Scherrer [53], the alternative hypothesis (H1: μ_X % $\neq$ μ_Y %) was assumed to be true when the main hypothesis (H0: $\mu_1 = \mu_2$) was rejected.

Results and discussion

Synthesis and characterization of HA DDS

HA/PMMA suspension was formed by mixing HA and PMMA dispersions. Heterocoagulation of both components was expected from electrostatic attraction between the oppositely charged nanometric HA particles and micrometric PMMA spheres. This was confirmed by observation of the mixture with SEM, which highlighted the formation of core/shell structures composed of PMMA microspheres covered by HA nanoparticles (Fig. 1c). After filtering to remove solvent, thermal treatments of the organic/inorganic composite were performed to remove PMMA particles and achieve sintering. Porous ceramics were obtained as final products. Figure 1d shows the typical porous structure of ceramics synthesized with a 0.42 HA/PMMA ratio and sintering temperature of 1220 °C (The micrograph was performed after fracture of a ceramic sample). Micropores are spread homogeneously in the material and are all interconnected. The spherical shape of PMMA spheres is preserved in the shape of the micropores.

Both porous ceramics used as HA matrices in the present work were obtained with shell-to-core ratio of 0.42. They differed in sintering temperature that was fixed at 1100 and 1220 °C for the so-called HA-1100 and HA-1220, respectively. As shown in Fig. 1e, characteristics of the matrix porosity vary accordingly to the sintering condition. The porogram also displays a low dispersion of pore and interconnection sizes for specific sintering condition. Porosity volume, pore and interconnection sizes resulting from the porosimetry analysis are summarized in Table 1. Pore size distribution is bimodal and trimodal in HA-1220 and HA-1100, respectively, and two populations of pores are shared by both HA matrices. On the basis of SEM micrographs, the population of pores with diameter from 2.3 to 10 μm can be attributed to the elimination of the porous agent i.e. PMMA microspheres. The second population with pore diameter in the [0.4–2.3 μm] range is attributed to interconnections with mean diameter of 1.1 μm for HA-1100 and 1.4 μm for HA-1220. The third population of pores was only highlighted in HA-1100 in a diameter range of [0.1–0.4 μm]. These pores only observed on SEM micrographs of HA-1100 and with a mean size of 0.2 μm were attributed to interconnections resulting from lower sintering temperature as compared to HA-1220. Additionally, porosity (72.5 %) and volume of interconnections (698 mm^3/g) were higher in HA-1100 than in HA-1220 (59.1 % and 438 mm^3/g), leading to less compactness of the pore walls in HA-1100 compared to HA-1220 (Fig. 1e). Sintering temperature was thus demonstrated to modulate the porosity and the size and volume of interconnections without changing size of PMMA microsphere and HA/PMMA ratio. Besides, measurement of HA material densification and subsequent calculation of the corresponding porosity of each sample used in the present work (mean values and standard deviations reported in Table 1) depicted a good reproducibility of the fabrication process, with a low relative variation of the porosity throughout the whole sample population

Table 1 Porosity characteristics of porous HA matrices (HA-1100 and HA-1220) obtained after sintering at temperature of 1100 and 1220 °C, respectively

	HA-1100	HA-1220
Calculated porosity[a] (%)	73.3 ± 1.3	65.7 ± 2.5
Measured porosity[b] (%)	72.5	59.1
Mean interconnection pore size (μm) in diameter range of [0.1–0.4 μm]	0.23	Multidisperse distribution (see Fig. 1)
Mean interconnection pore size (μm) in diameter range of [0.4–2.3 μm]	1.1	1.4
Mean porous volume (mm^3/g) in diameter range of [0.1–0.4 μm]	57	4
Mean porous volume (mm^3/g) in diameter range of [0.4–2.3 μm]	698	438

[a] Porosity was calculated on the basis of densification

[b] Porosity was measured by mercury porosimetry

compared to the mean value (1.8 and 3.8 % for HA-1100 and HA-1220, respectively).

TC-HA materials

TC quantities loaded in HA matrices for various concentrations of the loading TC solutions were determined by total dissolution of HA in acid solution (Fig. 2a). As expected, variation in loaded TC quantity was observed to follow HA matrix porosity: Matrix presenting higher porosity volume and more interconnections, as highlighted for TC-HA-1100, allowed the loading of higher quantities of TC compared to HA matrix with a more compact structure (TC-HA-1220). This is attributed to the higher surface of adsorption offered by the porosity and the interconnections of TC-HA-1100 in agreement with theoretical and experimental results reported in the literature [9, 16]. In addition, the loaded TC quantity increases linearly with TC concentration of the loading solution for both HA matrix types. Further antibacterial assays were conducted with TC-HA-1100 and TC-HA-1220 DDS of the lowest TC-loaded doses i.e. obtained by loading 5 mg/mL TC solutions in ethanol. Their corresponding doses of adsorbed TC, as determined by total TC-HA dissolution in acid and by TPD measurement, are reported in Table 2. Results of both methods are in very good accordance and confirm the higher quantity of TC loaded in TC-HA-1100 compared to TC-HA-1220.

The release properties of both TC-HA DDS types were compared for equal doses of adsorbed TC. Thus, kinetics of TC release were analysed for TC-HA-1100 and TC-HA-1220 samples loaded with 15 mg of TC per g of HA, obtained with impregnation with a TC solution of 10 and 15 mg/mL, respectively (Fig. 2a). Assays were conducted for 6 h in 50 mL of water (Fig. 2b). As determined before and reported in Table 2, loaded TC quantities were 0.44 ± 0.05 and 0.32 ± 0.07 mg for TC-HA-1100 and TC-HA-1220, respectively. Considering the total release of TC, maximal concentrations were equal to 0.008 and 0.006 mg/mL, broadly lower than the solubility of TC (33 mg/mL in water and for temperature of 15–25 °C). Therefore, SINK conditions were respected (medium volume $\gg 3\times$ volume at solubility limit) and the full dose of tetracycline was consequently allowed to be released. The structure of HA matrix was maintained throughout the release assays, demonstrating the stability of the DDS system (data not shown). For all the tested samples, 100 % of the total loaded quantity of TC was released throughout the assays, showing that the total release was achieved (Fig. 2b). In addition, two different regimes were distinguished in the kinetic curves, with a first, fast release of TC from DDS, up to 60 % of the total loaded quantity of TC (Region I in Fig. 2b), and, in a second time, a significantly slower release from DDS of TC molecules still entrapped in DDS ceramic matrix (Region II in Fig. 2b). The difference in release speed is attributed to the origin of the released TC molecules: Fast release, observed in region I and similar for the two samples, might be related to TC molecules adsorbed on the surface of pores directly open to the outer sides of the DDS sample, while slower release might result from TC molecules adsorbed in the porous HA material core. Such presence of TC in the internal pores is supported by optical micrographs of fractured DDS samples (Fig. 2c) that clearly show the capability of TC loading under vacuum conditions to drive TC molecules (here visible as yellow TC crystals) into the core of the DDS samples. Furthermore, the second region of the kinetics curve attributed to the porous core slightly but significantly differs between TC-HA-1100 and TC-HA-1220. T80 $\%_{1220}$(time necessary to release 80 % of TC loaded on HA-1220) is almost two times higher than T80 $\%_{1100}$(time necessary to release 80 % of TC loaded on HA-1100) (1.25 and 0.70 h, respectively), showing a faster release from TC-HA-1100 in agreement with more interconnections able to favour release of TC adsorbed in the material core. In comparison with other works on DDS such as Murugan et al. [54] and Domingues et al. [55], the release of TC appeared to be relatively fast. This can be explained by the experimental conditions that are

Table 2 Quantity of TC molecules loaded in HA matrix and determined both by TPD and by total releasing

	Value measured by TPD (in mg per g of HA)	Value measured by total dissolution (in mg per g of HA)	Value measured by total dissolution (in mg per sample)
TC-HA-1100	5.8 ± 1.6	6.9 ± 0.3	0.44 ± 0.05
TC-HA-1220	4.8 ± 0.1	5.0 ± 0.4	0.32 ± 0.07

known to directly impact release kinetics [56]. Indeed our priority was to study the effect of porosity on the kinetics using standardized experimental conditions and not to predict the in vivo release. Therefore, the choice was made to perform the trials in 50 mL of dissolution medium under agitation and to take aliquots for the TC dosage as a function of time. These conditions limit variations all along the duration of the release, but they can lead to a faster release of the drug substance in comparison with trials performed using dissolution medium volumes of a few mL. In addition, considering the notable difference in diffusion offered by biological tissues and biofilms compared to aqueous liquids [57–60], release kinetics of TC is expected to significantly slow down in in vivo conditions compared to in vitro ones [61, 62]. In vivo duration for total release should therefore finally continue far beyond the in vitro determined 6-h duration.

Bacterial growth inhibition

The efficiency of TC-HA DDS for preventing development of bacteria in its near surroundings i.e. resulting from TC molecules released and diffused in the liquid or semi-solid medium, was evaluated for planktonic bacteria living in liquid culture medium and for bacteria growing on semi-solid nutritive agar plates.

Significant inhibition of bacterial growth was observed in the presence of TC-HA DDS in both liquid and semi-solid culture media (Fig. 3), clearly highlighting that the TC efficiency was conserved after the loading and releasing processes. Inhibition areas were observed on the nutritive agar plates used for the diffusion assay, around both the TC-HA-1100 and the TC-HA-1220 samples placed top-down on the inoculated agar plates (Fig. 3a). The inhibition area was slightly higher with TC-HA-1100 (9.1 ± 1.3 cm^2) compared to TC-HA-1220 (8.4 ± 0.7 cm^2) in agreement with the higher amount of TC loaded in TC-HA-1100 (Table 2), but differences were not significant. The inhibition efficiency measured in liquid culture medium was determined by comparing the concentration of planktonic bacteria in 4 mL of culture medium in the presence of TC-HA (i.e. with TC concentration of 110 ± 12 and 80 ± 17 μg/mL, see Table 2) and HA samples for 2 h. Results shown in Fig. 3b display a reduction of more than 50 % of planktonic population growth in the surroundings of HA-TC DDS compared to HA DDS. Inhibition of bacteria growth was not significantly different between materials obtained with different sintering temperatures ($Inh_{plank1} = 51 \pm 8$ % for TC-HA-1100; $Inh_{plank1} = 53 \pm 1$ % for TC-HA-1220). In addition, inhibition rates were in accordance with the expected values (45 ± 5 % for 100 μg/mL of TC with pre-culture and culture in M63G; see Supporting Information, Fig. 3), knowing the maximal concentration of TC reached in 4 mL of M63G medium with one TC-HA DDS sample (110 and 80 μg/mL for TC-HA-1100 and TC-HA-1220 respectively). It should be noted that susceptibility of bacteria to antibacterial agent is strongly dependent on the growth conditions, especially on the composition of growth medium [63]. As we experimentally confirmed, inhibition rates in M63G medium are lower than in LB culture medium, commonly used in literature (about 80 % in LB medium supplemented with 100 μg/mL of TC) (Supporting Information, Fig. 3). Higher efficiency of TC-HA DDS can be therefore expected under in vivo conditions of use.

Kinetics of planktonic bacteria growth in the presence of TC-HA DDS was analysed for 7 days in 22 mL of liquid nutritive medium (Fig. 3c, d). For both DDS types, resulting inhibition rate displayed two regimes: inhibition rate increased rapidly up to about 60 % during the first 8 h, while it only slowly rises during the next 6 days, reaching about 85 % after 7 days of culture in the presence of TC-HA DDS (Fig. 3c). The rapid inhibition increase can be attributed to the high doses of TC released in culture medium during the first period (as reported above, in 50 mL of water, about 100 % of the loaded TC quantity in the 6 first hours) i.e. 0.020 and 0.015 g/L as estimated for TC-HA-1100 and TC-HA-1220, respectively. The inhibition rates reached after 2 h of culture were 45 ± 4 and 30 ± 6 % for TC-HA-1100 and TC-HA-1220, respectively, in accordance with the inhibition value (about 35 %) expected from similar TC concentrations and M63G culture medium (Supporting Information, Fig. 3). Besides, switching from lag to stationary bacterial growth phase after 8 h of culture may have led to a change in the bacterial susceptibility to the TC antibiotics, as it was already reported in the literature for many antibiotics classes [64–66]. This might have resulted in the loss of bacterial population observed in the presence of TC-HA DDS after 8 h of culture (Fig. 3d) and have thus

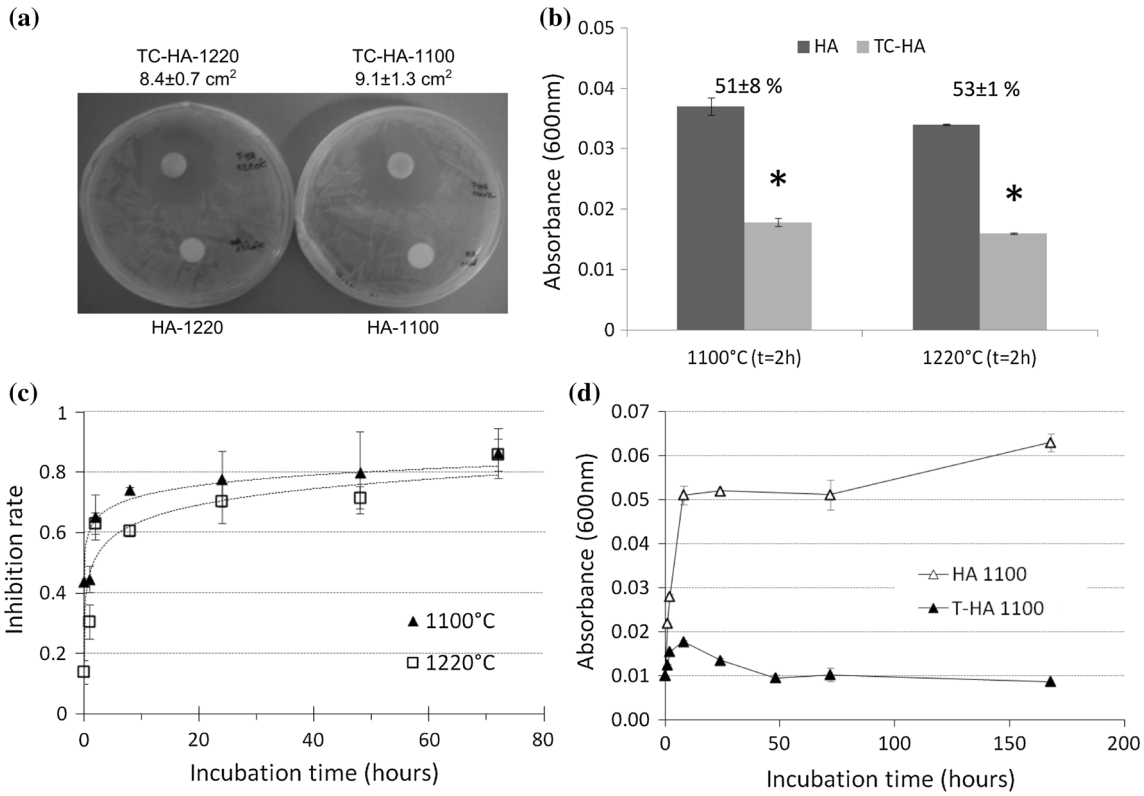

Figure 3 Antibacterial properties of HA and HA-TC DDS on bacteria living in the near material surroundings, on semi-solid nutritive agar plates (**a**) or in liquid culture medium (i.e. planktonic bacteria) (**b**, **c**). **a** Photographs of TC-HA and HA DDS samples placed onto agar inoculated plates ("diffusion test"). Measurements of inhibition areas around TC-HA-1100 and TC-HA-1220 DDS samples are reported. **b** Bacteria concentrations measured for HA-1100, HA-1220, TC-HA-1100, and TC-HA-1220 samples after 2 h of incubation in 4 mL of medium, and corresponding Inh_{plank1} inhibition rates. *significantly different from HA ($\alpha < 0.01$). **c** Kinetic evolution of bacterial growth inhibition resulting from TC-release calculated from bacteria concentrations measured for HA and TC-HA DDS samples after from 1 h to 1 week incubation time in 22 mL of liquid medium. **d** Evolution of bacteria population in the presence of HA-1100 and TC-HA-1100 DDS samples during 1 week (168 h).

provided the slight increase of inhibition highlighted in the second period of the experiment.

Inhibition rates measured throughout the kinetics experiments (Inh_{plank2}) reveal higher antimicrobial efficiency of TC-HA-1100 DDS than TC-HA-1220, confirming the results obtained on semi-solid nutritive medium but in contrast to measurements performed in 4 mL of liquid medium (Inh_{plank1}). The difference may result from the methodology used for sampling bacterial suspensions for further measurements of bacteria concentration. Indeed, the supernatants of samples incubated in 4 mL are almost completely removed through several rinsing, leading to harvesting quasi all non-adherent bacteria (Supporting Information, Fig. 2). In contrast, kinetics experiments consist in the removal of small volumes of the bacterial suspension at several specific times, leading to harvest the fraction of non-adherent bacteria population living in the close surroundings of the material surface e.g. non-adherent bacteria confined in the HA pores. In agreement, bacteria concentrations measured after 2 h of incubation in 4 mL medium are higher than those determined with the kinetics assay for all the HA-1100, HA-1220, TC-HA-1100 and TC-HA-1220 samples (Supporting Information, Table 1). In addition, bacteria concentrations are similar for HA-1100 and HA-1220 when measured in 4 mL assay, while they are in larger number with HA-1100 than with HA-1220 in kinetics experiments for the same incubation time. This difference between both types of HA matrix in the absence of rinsing steps suggests that bacteria free-living in the near material surroundings are in a higher amount with HA-1220 than with HA-1100, which may be

attributed to the difference in pore size of both matrices. Indeed, pore size in HA-1220 matrix (average of 1.4 μm) is in better accordance with *E. coli* size (~1 μm × 3 μm as reported in the literature [67] and 2.3 ± 0.5 μm × 1.4 ± 0.2 μm as measured by our group with fluorescence confocal microscope [68]) than in HA-1100 matrix (average of 1.1 μm) (Table 1). Based on the pore size distribution depicted in Fig. 1, it can be estimated that pores with diameter larger than 1.5 μm are rare in HA-1100 material but frequent (~50 % of all pores) in HA-1220 material. This may have enhanced the probability for bacteria to enter pores at the HA-1220 material surface compared to those present at the HA-1100 surface, in agreement with results already reported in the literature regarding impact of surface microtopography on bacterial retention [69–71].

Bacterial attachment

Effect of TC-loaded DDS on short-term material colonization by bacteria was assessed by confocal laser scanning microscopy both in reflection and in fluorescence modes. Bacteria were preferentially observed in pores, with individual bacteria being in topographic features with size similar to bacterial one (Fig. 4a) and bacterial colonies in pore with larger size (Fig. 4b). In accordance with the literature, this was attributed to the retention of individual adhered bacteria in the protected locations formed by pores fitting with the cell size [69, 72–74] and their potential proliferation until colonies were filling the confined space of the pores [74, 75]. This resulted in a heterogeneous distribution of bacteria throughout the samples, as displayed by the high deviation in the bacteria number values extracted from CLSM micrographs. In the antibacterial application point of view, this may compromise the colonization of material surface by the pioneer bacteria retained in pores by preventing the spreading of their clones as suggested by Huysman et al. and Wang et al. [74, 75]. In addition, amounts of adhered bacteria, determined after 2 h of incubation in culture medium on randomly chosen locations of the sample surfaces, show a colonization being significantly reduced on both TC-HA-1100 ($\alpha < 0.01$) and TC-HA-1220 DDS ($\alpha < 0.01$) compared to colonization on HA matrix without TC (Fig. 4c). This result agreed complementary assays consisting in harvesting adhered bacteria by printing the top side of DDS samples onto an agar nutritive plate (Supporting Information, Fig. 4). On the other hand, variations of up to 41 % of the surface concentration were observed on CLSM micrographs between samples of the same material type, probably resulting from the high heterogeneity of colonization already reported and leading to high deviations in the inhibition rates determined for both HA-1100 and HA-1220 materials (Supporting Information, Table 1). Despite of this reservation, however, the quantity of TC that was loaded in HA-1100 and HA-1220 matrices was shown to be in capacity to inhibit 56 ± 34 and 30 ± 18 % of bacterial adhesion, respectively.

HA-1100 and HA-1220 DDS did not differ in term of bacteria amount adhered on their surface. This suggests that, even if difference in pore size of HA-1100 and HA-1220 may have affected confinement of planktonic bacteria in pores as discussed above, the slightly higher population confined in HA-1220 pores compared to HA-1100 pores was not sufficient to significantly affect the extend of short-term colonization on DDS. In contrast, the reduction in bacterial colonization provided by TC-loaded DDS compared to TC-free DDS differed according to the HA matrix type. Colonization was significantly less on TC-HA-1100 than on TC-HA-1220 DDS, in agreement with the loaded quantity of TC and in accordance to the higher inhibition effect provided by TC-HA-1100 DDS onto planktonic bacteria compared to TC-HA-1220 DDS.

Protein adsorption

Biomolecules of the cell culture medium were expected to adsorb onto DDS and to potentially affect release and antibacterial properties of the DDS. This was tested during perfusion in adequate bioreactors [50]. XPS analysis of the ceramics sample surfaces, performed before and after perfusion in bioreactors, demonstrated the formation of a protein coating, which led to hide the originate composition of the sample surface characterized by Ca2*p*%, P2*p*% and O1*s*% components (Supporting Information, Table 2). Weak quantities of N1*s*%, Na1*s*% and Cl2*p*% components detected on TC-HA samples before protein adsorption were attributed to TC and its initial buffer, while the slight increases of Na1*s*% and Cl2*p*% components on HA samples after perfusion experiments were attributed to mineral constituents of the culture medium used for adsorption experiments. In the same time, surface content in C1*s*% and N1*s*%

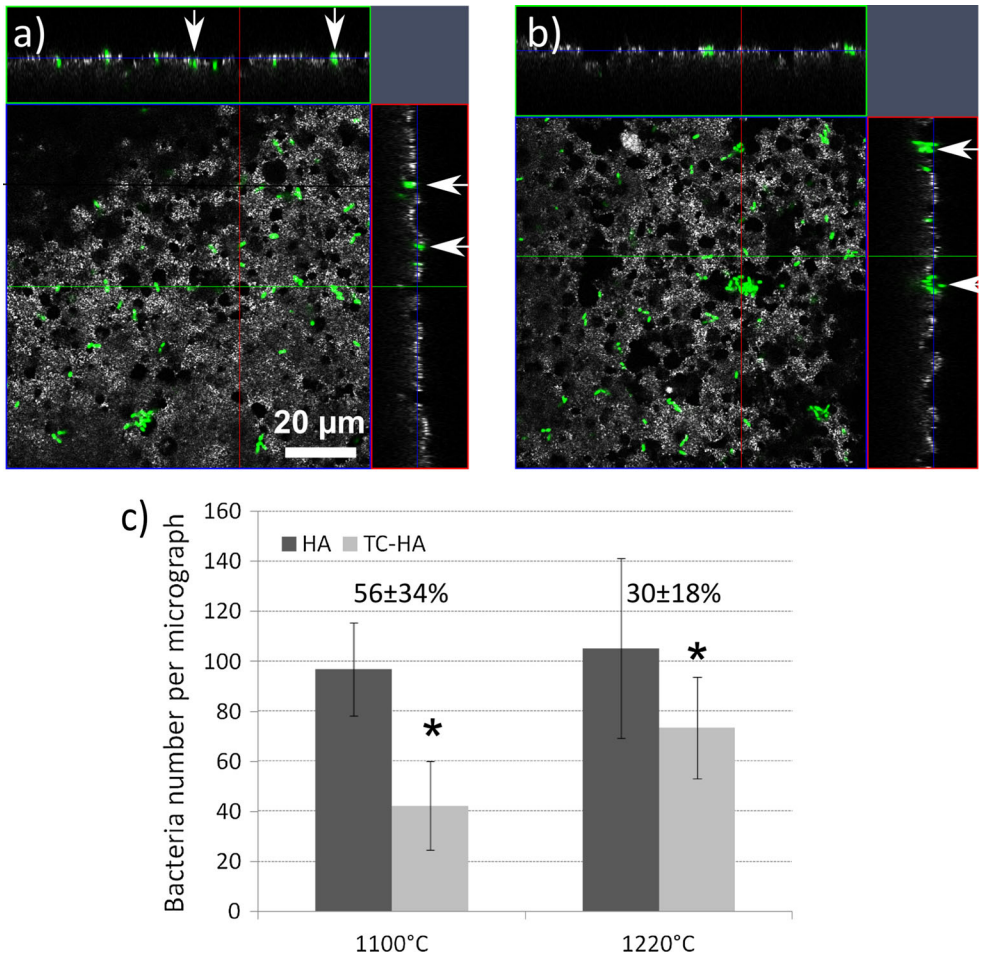

Figure 4 Colonization of HA and TC-HA DDS samples after 2 h of incubation in culture medium. **a** CLSM image showing HA material surface and bacterial colonization observed by reflection and fluorescence modes. Bacteria were labelled using Syto9® (Molecular Probes) prior to observation. White arrows show single cells (**a**) and bacterial colonies (**b**) in topographical features of different sizes. **c** Number of adherent bacteria, and corresponding Inh_{adh} inhibition rate, determined by image analysis on CLSM micrographs. Bacteria were labelled using Syto9® (Molecular Probes) prior to observation. Image treatment and image analysis were conducted with ImageJ [47] and CellC software [48], respectively. *significantly different from corresponding HA ($\alpha < 0.01$).

Table 3 Amounts of protein adsorbed on porous HA and TC-HA DDS samples after perfusion with cell culture medium in bioreactors

	HA-1100	HA-1220	TC-HA-1100	TC-HA-1220
Amount of proteins adsorbed per sample (~65 mg of HA)	5 ± 3 mg	3 ± 2 mg	5 ± 3 mg	3 ± 1 mg

components raises in agreement with the presence of biological organic compounds such as proteins.

Quantity of adsorbed proteins was indirectly evaluated by dosing proteins of the culture medium before and after perfusion of HA and TC-HA materials. Similar amounts of adsorbed proteins were measured for HA and the corresponding TC-HA material showing that protein adsorption was not significantly affected by the presence of TC on the DDS surface (Table 3). Ranging from 45 to 75 mg of proteins per g of HA, they are in agreement with results previously reported for BSA used at similar concentrations as in the present study (i.e. about 2 mg/mL as compared to 10 % FBS in the culture medium) [76–78]. Furthermore, significantly more proteins were adsorbed on HA-1100 and TC-HA-

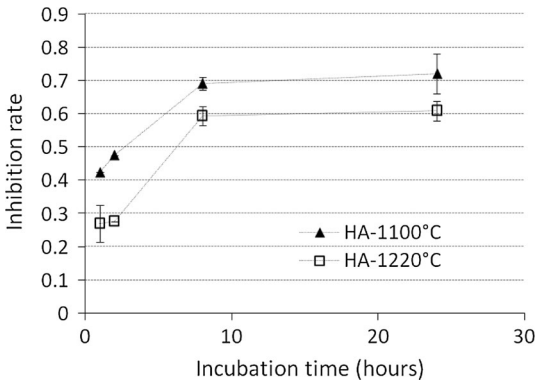

Figure 5 Growth inhibition rates of TC-HA-1100 and TC-HA-1220 materials after previous adsorption of proteins realized in perfusion bioreactors. Concentrations of bacteria were measured in 22 mL medium for 1, 2, 8 and 24 h.

1100 compared to HA-1220 and TC-HA-1220. This is consistent with the higher porosity and porous volume measured in HA-1100 materials compared to HA-1220 ones, which is expected to favour the adsorption of a larger amount of proteins in HA-1100 derived-DDS due to more surface area exposed to proteins [14, 79].

Antibacterial efficiencies onto planktonic bacteria were not modified after adsorption of proteins. They were measured for incubation times from 1 to 24 h for both HA-1100 and HA-1220 matrices, resulting in inhibition rates of planktonic bacteria equivalent to without protein adsorption (Fig. 5) and reaching about 70 and 60 % after 24 h of culture for HA-1100 and HA-1220, respectively. As for materials without protein conditioning, and despite more proteins adsorbed on HA-1100 DDS samples, HA-1100-based DDS offered higher inhibition efficiency on planktonic bacterial population compared to HA-1220 DDS. This may be explained by the presence of proteins adsorbed as aggregates rather than continuous layer as it has been already reported in the literature [78]. Proteins might not completely screen the HA surface and therefore might only slightly or even not prevent the release of TC. Such slight changes in the TC concentration released from DDS may lead to weak, undetectable changes in the bacterial growth.

Finally, TC-HA-1100 matrix was showed to uptake higher doses of TC and to release them in a faster way than TC-HA-1220 matrix, in agreement with the porous structure and especially in relation with the presence of pore interconnections. Accordingly, TC-HA-1100 DDS displayed better antibacterial properties than TC-HA-1220 DDS in terms of the inhibition of bacteria growth, both in suspension and for bacteria adhered on the material. Nevertheless, and in spite of its satisfying stability observed during the physical–chemical and antibacterial characterization studies, TC-HA-1100 displayed a higher sensitivity to multiple manipulations than TC-HA-1220, due to the weaker resistance to mechanical strains of pore walls, enriched in interconnections and therefore less cohesive compared to HA-1220 bioceramic. Accordingly, TC-HA-1220 DDS were preferred for the experiments with mammalian cells and, further, for applications in in vivo conditions.

In vitro biocompatibility for eukaryotic cells

Biocompatibility of HA and TC-HA DDS was tested by culturing MC3T3-E1 cells in media previously immersing DDS samples for 5 days (i.e. allowing total TC release). Proliferation of MC3T3-E1 cells in material-free media was similar to both extraction media of the positive control (i.e. Thermanox® coverslip) and media extracted from HA and TC-HA DDS (Fig. 6a), clearly demonstrating the absence of in vitro toxicity of the quantity of TC released from TC-HA DDS.

Cell adhesion and proliferation on both HA and TC-HA DDS were also investigated by analysing cell number, viability and morphology (cell area and cell circularity) after 6, 24 and 72 h of culture on the DDS samples (Fig. 6b, c). CLSM micrographs display slightly less adhered cells on HA and TC-HA compared to positive control (Fig. 6d), which is attributed to the surface morphology of the porous HA matrices in agreement to results reported in the literature regarding cell adhesion and proliferation on microstructured surfaces compared to flat surfaces [80]. In contrast, chemical properties of HA are known to be favourable to cell attachment and development [81]. The slightly less quantity of cells was accompanied by the reduction of cell size on HA and TC-HA compared to positive control (Fig. 6e) but similar cell viability and circularity (Fig. 6d, e), suggesting impact of the surface morphology onto cell spreading without any significant cytotoxic effect of the material. Accordingly, number, viability, size and circularity of cells were significantly different on the negative control.

Importantly, any difference was observed between HA and TC-HA DDS in terms of number, size,

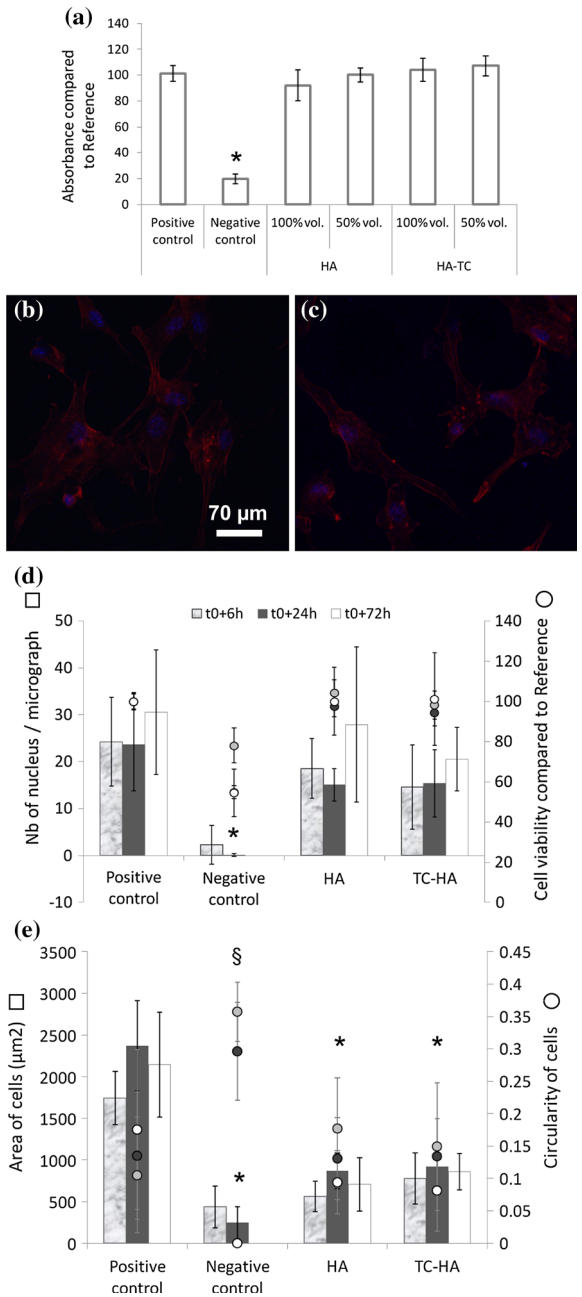

Figure 6 In vitro biocompatibility of HA-1220 and TC-HA-1220 (4.2 ± 0.8 mg TC/g HA) DDS samples. **a** MC3T3-E1 cell proliferation in extraction media of positive control (Thermanox®), negative control (Phenol 25 %), HA and TC-HA DDS compared to fresh medium without material (Reference). *significantly different to Reference ($\alpha < 0.01$). **b**, **c** CLSM micrographs of MC3T3-E1 cell after 24 h culture on HA and TC-HA DDS samples, respectively. **d** Number of cell nucleus and cell viability as determined on CLSM micrographs and by PrestoBlue® labelling, respectively. **e** Average area and circularity of cells as determined on CLSM micrographs. * and § significantly different to Positive control, for *bars* and *circles*, respectively ($\alpha < 0.01$).

circularity and viability of cells, demonstrating the in vitro compatibility of the TC-loaded quantity with the tested eukaryotic cells. This is in agreement with results reported in the literature for similar quantities of TC on mesenchymal cells comparable to MC3T3-E1 cells [82].

Finally, the present results demonstrate the possibility to provide and control antibacterial effects of antibiotics- and HA-bioceramics-based DDS whilst maintaining biocompatible properties for eukaryotic cells. Nevertheless, since anti-infectious efficiency of similar quantities of TC is expected to be modified i.e. reduced in real in vivo conditions of use and even if good accordance of efficient doses in in vivo and in vitro conditions has already been reported in the literature [1, 83], TC quantity in DDS will probably need to be adapted for in vivo use to fit the necessary, favourable antibacterial versus biocompatible properties balance. In vivo studies with this aim are currently under development. Also aiming at the improvement of the DDS performance in in vivo conditions of use, similar DDS with other antibiotics such as vancomycin are under investigation.

Conclusion

New antibiotics DDS based on HA ceramic matrix of controlled porosity were successfully developed by a colloidal heterocoagulation approach using hydroxyapatite nanoparticles and polymethylmethacrylate microspheres. With constant size of microspheres and HA/PMMA ratio, the sintering temperature allowed the modulation of interconnections porosity and volume, then allowing the loading of antibiotics in quantity dependent on matrix porosity. The release and antibacterial properties of DDS of two different porosities were investigated, demonstrating the possibility to control the loaded quantity of antibiotics, and therefore their antibacterial efficiency by varying the matrix porosity. Release kinetics is also slightly affected by changes in ceramic porosity, given the moderate porosity differences induced by varying the sintering temperature. DDS loaded with TC were also shown to provide biocompatible properties for MC3T3 eukaryotic cells in in vitro conditions. Adaptation of TC-loaded quantities for use in in vivo conditions is the subject of further investigations. In addition, similar DDS with alternative antibiotics are currently under evaluation in in vivo conditions.

Acknowledgements

All works done at the Institut de Science des Matériaux de Mulhouse were funded by the French "Centre National de la Recherche Scientifique" (CNRS). The present project was also especially funded by Agence Nationale de la Recherche (ANR, France) in the frame of the BiocerPorDDS2 project. In addition, the authors sincerely thank Dr Corinne Dorel and Pr Philippe Lejeune for *E. coli* strain, Dr Arnaud Ponche for XPS analyses and Dr Loic Vidal for SEM analyses reported in Supporting Information. The authors also dedicate this article to Dr Roxana Chotard-Ghodsnia, who initiated the project and invested in it her enthusiasm and energy. Dr. Roxana Chotard-Ghodsnia was deceased at the time of writing the manuscript.

Electronic supplementary material: The online version of this article (doi:10.1007/s10853-016-0133-z) contains supplementary material, which is available to authorized users.

References

[1] McCann M, Gilmore B, Gorman S (2008) Staphylococcus epidermidis device-related infections: pathogenesis and clinical management. J Pharm Pharmacol 60(12):1551–1571

[2] Costerton JW, Stewart PS, Greenberg EP (1999) Bacterial biofilms: a common cause of persistent infections. Science 284(5418):1318–1322

[3] Saito T, Takeuchi R, Hirakawa K, Nagata N, Yoshida T, Koshino T, Okuda K, Takema M, Hori T (2002) Slow-releasing potential of vancomycin-loaded porous hydroxyapatite blocks implanted into MRSA osteomyelitis. J Biomed Mater Res B 63:245–251

[4] Pataro A, Franco C, Santos V, Cortes M, Sinisterra R (2003) Surface effects and desorption of tetracycline supramolecular complex on bovine dentine. Biomaterials 24:1075–1080

[5] Gbureck U, Vorndran E, Muller F, Barralet J (2007) Low temperature direct 3D printed bioceramics and biocomposites as drug release matrices. J Controlled Release 122:173–180

[6] Castro C, Sanchez E, Delgado A, Soriano I, Nunez P, Baro M, Perera A, Evora C (2003) Ciprofloxacin implants for bone infection: in vitro–in vivo characterization. J Controlled Release 93:341–354

[7] Descamps M, Hornez J, Leriche A (2009) Manufacture of hydroxyapatite beads for medical applications. J Eur Ceram Soc 29(3):369–375

[8] Laurent F, Bignon A, Goldnadel J, Chevalier J, Fantozzi G, Viguier E, Roger T, Boivin G, Hartmann D (2008) A new concept of gentamicin loaded HAP/TCP bone substitute for prophylactic action: in vitro release validation. J Mater Sci: Mater Med 19(2):947–951

[9] Espanol M, Perez RA, Montufar EB, Marichal C, Sacco A, Ginebra MP (2009) Intrinsic porosity of calcium phosphate cements and its significance for drug delivery and tissue engineering applications. Acta Biomater 5:2752–2762

[10] Hasegawa M, Sudo A, Komlev V, Barinov S, Uchida A (2004) High release of antibiotic from a novel hydroxyapatite with bimodal pore size distribution. J Biomed Mater Res B Appl Biomater 70B:332–339

[11] Slosarczyk A, Szymura-Oleksiak J, Mycek B (2000) The kinetics of pentoxifylline release from drug-loaded hydroxyapatite implants. Biomaterials 21:1215–1221

[12] Sunder M, Ramesh Babu N, Prem Victor S, Ram Kumar K, Sampath Kumar TS (2005) Biphasic calcium phosphates for antibiotic release. Trends Biomater Artif Organs 18(2):213–218

[13] Palazzo B, Sidoti MC, Roveri N, Tampieri A, Sandri M, Bertolazzi L, Galbusera F, Dubini G, Vena P, Contro R (2005) Controlled drug delivery from porous hydroxyapatite grafts: an experimental and theoretical approach. Mater Sci Eng C 25:207–213

[14] Arcos D, Vallet-Regi M (2013) Bioceramics for drug delivery. Acta Mater 61:890–911

[15] Ginebra MP, Traykova T, Planell JA (2006) Calcium phosphate cements: competitive drug carriers for the musculoskeletal system? Biomaterials 27:2171–2177

[16] Gbureck U, Vorndran E, Müller FA, Barralet JE (2007) Low temperature direct 3D printed bioceramics and biocomposites as drug release matrices. J Controlled Release 122:1736180

[17] Meurice E, Leriche A, Hornez J-C, Bouchart F, Rguiti E, Boilet L, Descamps M, Cambier F (2012) Functionalisation of porous hydroxyapatite for bone substitutes. J Eur Ceram Soc 32:2673–2678

[18] Wang W, Chu B, Lin C, Chen S, Ru H, Yue X, Jia Q (2014) Preparation of 3D interconnected macroporous hydroxyapatite scaffolds by PVA assisted foaming method. Ceram Int 40:1789–1796

[19] Butscher A, Bohner M, Hofmann S, Gauckler L, Müller R (2011) Structural and material approaches to bone tissue engineering in powder-based three-dimensional printing. Acta Biomater 7:907–920

[20] Bose S, Vahabzadeh S, Bandyopadhyay A (2013) Bone tissue engineering using 3D printing. Mater Today 16(12):497–504

[21] Chevalier E, Chulia D, Pouget C, Viana M (2008) Fabrication of porous substrates: a review of processes using pore forming agents in the biomaterial field. J Pharm Sci 97:1135–1154

[22] Studart A, Gonzenbach U, Tervoort E, Gauckler L (2006) Processing routes to macroporous ceramics: a review. J Am Ceram Soc 89:1771–1789

[23] Destainville A (2005) Etude du phosphate tricalcique, application à l'élaboration de biomatériaux céramiques macroporeux en phosphates de calcium. University of Limoges France

[24] Krajewski A, Ravaglioli A, Roncari E, Pinasco P, Montanari L (2000) Porous ceramic bodies for drug delivery. J Mater Sci Mater Med 12:763–771

[25] Komlev VS, Barinov SM, Koplik EV (2002) A method to fabricate porous spherical hydroxyapatite granules intended for time-controlled drug release. Biomaterials 23:3449–3454

[26] Descamps M, Hornez JC, Leriche A (2009) Manufacture of hydroxyapatite beads for medical applications. J Eur Ceram Soc 29:369–375

[27] Cyster LA, Grant DM, Howdle SM, Rose FRAJ, Irvine DJ, Freeman D, Scotchford CA, Shakesheff KM (2005) The influence of dispersant concentration on the pore morphology of hydroxyapatite ceramics for bone tissue engineering. Biomaterials 26:697–702

[28] Jones JR, Ehrenfried LM, Hench LL (2006) Optimising bioactive glass scaffolds for bone tissue engineering. Biomaterials 27:964–973

[29] Chotard-Ghodsnia R, Lucas S, Pagnoux C, Champion E, Viana M, Chulia D, Anselme K, Chartier T (2009) Elaboration of a well-ordered porous bioceramic via a heterocoagulation colloidal process. Key Eng Mater 396:515–518

[30] Tang F, Fudouzi H, Uchikoshi T, Sakka Y (2004) Preparation of porous materials with controlled pore size and porosity. J Eur Ceram Soc 24:341–344

[31] Guichaoua L, Chotard-Ghodsnia R, Viana M, Pagnoux C, Champion E, Chulia D, Chartier T (2009) Microporous hydroxyapatite elaborated through colloidal processing for drug loading and release. In: M. Bucko KH, Z. Pedzich and L. Zych (eds) 11th International Conference and Exhibition of the European Ceramic Society, Krakow

[32] Pecqueux F, Tancret F, Payraudeau N, Bouler JM (2010) Influence of microporosity and macroporosity on the mechanical properties of biphasic calcium phosphate bioceramics: modelling and experiment. J Eur Ceram Soc 30:819–829

[33] Park YJ, Lee YM, Park SN, Lee JY, Ku Y, Chung CP, Lee SJ (2000) Enhanced guided bone regeneration by controlled tetracycline release from poly(L-lactide) barrier membranes. J Biomed Mater Res Part B 51:391–397

[34] Schmidt D, Waldeck H, Kao W (2009) Protein adsorption to biomaterials. In: Puleo DA, Bizios R (eds) Biological interactions on materials surfaces. Springer, US, pp 1–18. doi:10.1007/978-0-387-98161-1_1

[35] Raynaud S, Champion E, Bernache-Assollant D, Thomas P (2002) Calcium phosphate apatites with variable Ca/P atomic ratio I. Synthesis, characterisation and thermal stability of powders. Biomater Sci 23:1065–1072

[36] Fernandez H, Miller M (1998) Toxicilogical evaluation of certain veterinary drug residues in food—WHO food additives series 41. World Health Organization/US Food and Drug Administration, International Programme on Chemical Safety, Geneva

[37] Gadiou R, dos Santos EA, Vijayaraj M, Anselme K, Dentzer J, Soares GA, Vix-Guterl C (2009) Temperature-programmed desorption as a tool for quantification of protein adsorption capacity in micro- and nanoporous materials. Colloids Surf B 73(2):168–174. doi:10.1016/j.colsurfb.2009.05.012

[38] Halling-Sørensen B, Sengeløv G, Tjørnelund J (2002) Toxicity of tetracyclines and tetracycline degradation products to environmentally relevant bacteria, including selected tetracycline-resistant bacteria. Arch Environ Contam Toxicol 42(3):263–271. doi:10.1007/s00244-001-0017-2

[39] Aly AAM, Osman AH, Abo El-Maali N, Al-Hazmi GAA (2005) Thermal decomposition of tetracycline and cephalosporins metal complexes. Bull Pharm Sci 28(2):269–276

[40] Jeong J, Song W, Cooper WJ, Jung J, Greaves J (2010) Degradation of tetracycline antibiotics: mechanisms and kinetic studies for advanced oxidation/reduction processes. Chemosphere 78(5):533–540. doi:10.1016/j.chemosphere.2009.11.024

[41] Kamel AM, Fouda HG, Brown PR, Munson B (2002) Mass spectral characterization of tetracyclines by electrospray ionization, H/D exchange, and multiple stage mass spectrometry. J Am Soc Mass Spectrom 13(5):543–557. doi:10.1016/S1044-0305(02)00356-2

[42] Campoccia D, Montanaro L, Arciola CR (2006) The significance of infection related to orthopedic devices and issues of antibiotic resistance. Biomaterials 27(11):2331–2339

[43] Roggenkamp A, Sing A, Hornef M, Brunner U, Autenrieth I, Heesemann J (1998) Chronic prosthetic hip infection caused by a small-colony variant of *Escherichia coli*. J Clin Microbiol 36(9):2530–2534

[44] Tattevin P, Crémieux A-C, Pottier P, Huten D, Carbon C (1999) Prosthetic joint infection: when can prosthesis salvage be considered? Clin Infect Dis 29:292–295

[45] Vidal O, Longin R, Prigent-Combaret C, Dorel C, Hooreman M, Lejeune P (1998) Isolation of an *Escherichia coli* K-12 mutant strain able to form biofilms on inert surfaces: involvement of a new ompR allele that increases curli expression. J Bacteriol 180(9):2442–2449

[46] Anselme K, Davidson P, Popa AM, Giazzon M, Liley M, Ploux L (2011) Response to comment on "The interaction of cells and bacteria with surfaces structures at the nanoscale". Acta Biomater 7(4):1936–1937. doi:10.1016/j.actbio.2010.12.002

[47] Rasband W (1997) U. S. National Institutes of Health, Bethesda, Maryland, USA (1997) ImageJ

[48] Selinummi J, Seppälä J, Yli-Harja O, Puhakka J (2005) Software for quantification of labeled bacteria from digital microscope images by automated image analysis. Biotechniques 39:859–863

[49] Bonev B, Hooper J, Parisot J (2008) Principles of assessing bacterial susceptibility to antibiotics using the agar diffusion method. J Antimicrob Chemother 61(6):1295–1301. doi:10.1093/jac/dkn090

[50] Wang Y, Uemura T, Dong J, Kojima H, Tanaka J, Tateishi T (2003) Application of perfusion culture system improves in vitro and in vivo osteogenesis of bone marrow-derived osteoblastic cells in porous ceramic materials. Tissue Eng 9(6):1205–1214

[51] Mosmann T (1983) Rapid colorimetric assay for cellular growth and survival: application to proliferation and cytotoxicity assays. J Immunol Methods 65(1):55–63. doi:10.1016/0022-1759(83)90303-4

[52] Larson EM, Doughman DJ, Gregerson DS, Obritsch WF (1997) A new, simple, nonradioactive, nontoxic in vitro assay to monitor corneal endothelial cell viability. Invest Ophthalmol Vis Sci 38(10):1929–1933

[53] Scherrer B (2007) Biostatistique, vol 1. Gaëtan Morin éditeur - Les Editions de la Chenelière inc.

[54] Murugan R, Ramakrishna S (2004) Coupling of therapeutic molecules onto surface modified coralline hydroxyapatite. Biomaterials 25(15):3073–3080. doi:10.1016/j.biomaterials.2003.09.089

[55] Domingues ZR, Cortés ME, Gomes TA, Diniz HF, Freitas CS, Gomes JB, Faria AMC, Sinisterra RD (2004) Bioactive glass as a drug delivery system of tetracycline and tetracycline associated with β-cyclodextrin. Biomaterials 25(2):327–333. doi:10.1016/S0142-9612(03)00524-6

[56] Gbureck U, Vorndran E, Barralet JE (2008) Modeling vancomycin release kinetics from microporous calcium phosphate ceramics comparing static and dynamic immersion conditions. Acta Biomater 4(5):1480–1486. doi:10.1016/j.actbio.2008.02.027

[57] Galambos P, Forster FK (1998) Micro-fluidic diffusion coefficient. In: Micro Total Analysis Systems'98 Workshop (μTAS'98) Banff, Canada, pp 189–191

[58] de Beer D, Stoodley P, Lewandowski Z (1997) Measurement of local diffusion coefficients in biofilms by microinjection and confocal microscopy. Biotechnol Bioeng 53(2):151–158. doi:10.1002/(sici)1097-0290(19970120)53:2<151:aid-bit4>3.0.co;2-n

[59] Fatin-Rouge N, Starchev K, Buffle J (2004) Size effects on diffusion processes within agarose gels. Biophys J 86(5):2710–2719

[60] Sanders NN, De Smedt SC, Demeester J (2000) The physical properties of biogels and their permeability for macromolecular drugs and colloidal drug carriers. J Pharm Sci 89(7):835–849. doi:10.1002/1520-6017(200007)89:7<835:aid-jps1>3.0.co;2-6

[61] Kundu B, Soundrapandian C, Nandi SK, Mukherjee P, Dandapat N, Roy S, Datta BK, Mandal TK, Basu D, Bhattacharya RN (2010) Development of new localized drug delivery system based on ceftriaxone–sulbactam composite drug impregnated porous hydroxyapatite: a systematic approach for in vitro and in vivo animal trial. Pharm Res 27(8):1659–1676. doi:10.1007/s11095-010-0166-y

[62] Winne D, Verheyen W (1990) Diffusion coefficient in native mucus gel of rat small intestine. J Pharm Pharmacol 42(7):517–519. doi:10.1111/j.2042-7158.1990.tb06611.x

[63] Fass RJ, Barnishan J (1979) Effect of divalent cation concentrations on the antibiotic susceptibilities of nonfermenters other than *Pseudomonas aeruginosa*. Antimicrob Agents Chemother 16(4):434–438

[64] Eng RH, Padberg FT, Smith SM, Tan EN, Cherubin CE (1991) Bactericidal effects of antibiotics on slowly growing and nongrowing bacteria. Antimicrob Agents Chemother 35(9):1824–1828

[65] Mascio CTM, Alder JD, Silverman JA (2007) Bactericidal action of daptomycin against stationary-phase and nondividing Staphylococcus aureus cells. Antimicrob Agents Chemother 51(12):4255–4260. doi:10.1128/aac.00824-07

[66] Stewart PS (2002) Mechanisms of antibiotic resistance in bacterial biofilms. Int J Med Microbiol 292:107–113

[67] Reshes G, Vanounou S, Fishov I, Feingold M (2008) Cell shape dynamics in *Escherichia coli*. Biophys J 94(1):251–264. doi:10.1529/biophysj.107.104398

[68] Böhmler J, Haidara H, Ponche A, Ploux L (2015) Impact of chemical heterogeneities of surfaces on colonization by bacteria. ACS Biomater Sci Eng 1(8):693–704. doi:10.1021/acsbiomaterials.5b00151

[69] Whitehead KA, Colligon J, Verran J (2005) Retention of microbial cells in substratum surface features of micrometer

and sub-micrometer dimensions. Colloids Surf B 41(2–3):129–138

[70] Whitehead KA, Verran J (2006) The effect of surface topography on the retention of microorganisms. Trans IChemE, Part C, Food Bioprod Process 84(4):253–259

[71] Samonin VV, Elikova EE (2004) A study of the adsorption of bacterial cells on porous materials. Microbiology 73(6):696–701. doi:10.1007/s11021-005-0011-1

[72] Ge X, Leng Y, Lu X, Ren F, Wang K, Ding Y, Yang M (2015) Bacterial responses to periodic micropillar array. J Biomed Mater Res Part A 103(1):384–396. doi:10.1002/jbm.a.35182

[73] Verran J, Jackson S, Coulthwaite L, Scallan A, Loewy Z, Whitehead K (2014) The effect of dentifrice abrasion on denture topography and the subsequent retention of microorganisms on abraded surfaces. J Prosthet Dent 112(6):1513–1522. doi:10.1016/j.prosdent.2014.05.009

[74] Huysman P, Van Meenen P, Van Assche P, Verstraete W (1983) Factors affecting the colonization of non porous and porous packing materials in model upflow methane reactors. Biotechnol Lett 5(9):643–648. doi:10.1007/bf00130849

[75] Wang Y, da Silva Domingues JF, Subbiahdoss G, van der Mei HC, Busscher HJ, Libera M (2014) Conditions of lateral surface confinement that promote tissue-cell integration and inhibit biofilm growth. Biomaterials 35(21):5446–5452. doi:10.1016/j.biomaterials.2014.03.057

[76] Lindl T (2002) Zell- und Gewebekultur, 5th edn. Spektrum Akademischer Verlag, Heidelberg

[77] Gstraunthaler G (2003) Alternatives to the use of fetal bovine serum: serum-free Cell Culture. Altex 20:275–281

[78] Mavropoulos E, Costa AM, Costa LT, Achete CA, Mello A, Granjeiro JM, Rossi AM (2011) Adsorption and bioactivity studies of albumin onto hydroxyapatite surface. Colloids Surf B 83(1):1–9. doi:10.1016/j.colsurfb.2010.10.025

[79] Wang K, Zhou C, Hong Y, Zhang X (2012) A review of protein adsorption on bioceramics. Interface Focus 2(3):259–277. doi:10.1098/rsfs.2012.0012

[80] Deligianni DD, Katsala ND, Koutsoukos PG, Missirlis YF (2000) Effect of surface roughness of hydroxyapatite on human bone marrow cell adhesion, proliferation, differentiation and detachment strength. Biomaterials 22(1):87–96. doi:10.1016/S0142-9612(00)00174-5

[81] dos Santos EA, Farina M, Soares GA, Anselme K (2009) Chemical and topographical influence of hydroxyapatite and β-tricalcium phosphate surfaces on human osteoblastic cell behavior. J Biomed Mater Res Part A 89A(2):510–520. doi:10.1002/jbm.a.31991

[82] Bettany JT, Wolowacz RG (1998) Tetracycline derivatives induce apoptosis selectively in cultured monocytes and macrophages but not in mesenchymal cells. Adv Dent Res 12(1):136–143. doi:10.1177/08959374980120010901

[83] Kelm J, Regitz T, Schmitt E, Jung W, Anagnostakos K (2006) In vivo and in vitro studies of antibiotic release from and bacterial growth inhibition by antibiotic-impregnated polymethylmethacrylate hip spacers. Antimicrob Agents Chemother 50(1):332–335. doi:10.1128/aac.50.1.332-335.2006